



**HAL**  
open science

## **pH-responsive nano-structured membranes prepared from oppositely charged block copolymer nanoparticles and iron oxide nanoparticles**

Ujala Farooq, Lakshmeesha Upadhyaya, Ahmad Shakeel, Gema Martinez, M. Semsarilar

### **► To cite this version:**

Ujala Farooq, Lakshmeesha Upadhyaya, Ahmad Shakeel, Gema Martinez, M. Semsarilar. pH-responsive nano-structured membranes prepared from oppositely charged block copolymer nanoparticles and iron oxide nanoparticles. *Journal of Membrane Science*, 2020, 611, pp.118181. 10.1016/j.memsci.2020.118181 . hal-03005854

**HAL Id: hal-03005854**

**<https://hal.science/hal-03005854>**

Submitted on 15 Nov 2020

**HAL** is a multi-disciplinary open access archive for the deposit and dissemination of scientific research documents, whether they are published or not. The documents may come from teaching and research institutions in France or abroad, or from public or private research centers.

L'archive ouverte pluridisciplinaire **HAL**, est destinée au dépôt et à la diffusion de documents scientifiques de niveau recherche, publiés ou non, émanant des établissements d'enseignement et de recherche français ou étrangers, des laboratoires publics ou privés.

# 1        **pH-Responsive Nano-Structured Membranes Prepared from Oppositely** 2        **Charged Block Copolymer Nanoparticles and Iron Oxide Nanoparticles**

3        *Ujala Farooq<sup>a,§</sup>, Lakshmeesha Upadhyaya<sup>a,†</sup>, Ahmad Shakeel<sup>b</sup>, Gema Martinez<sup>c,d</sup>, Mona*  
4        *Semsarilar<sup>a,\*</sup>*

5        <sup>a</sup> Institut Européen des Membranes, IEM, UMR 5635, Univ. Montpellier, CNRS, ENSCM, Montpellier, France.

6        <sup>b</sup> Faculty of Civil Engineering and Geosciences, Delft University of Technology, the Netherlands.

7        <sup>c</sup> Networking Research Centre on Bioengineering, Biomaterials and Nanomedicine, CIBER-BBN, 28029  
8        Madrid, Spain.

9        <sup>d</sup> Department of Chemical and Environmental Engineering and Aragon Nanoscience Institute, Campus Río  
10        Ebro, C/ Mariano Esquillor s/n ,50018 Zaragoza, Spain.

11        \* Corresponding author

12        Current address:

13        <sup>§</sup> Faculty of Aerospace Engineering, Delft University of Technology, the Netherlands.

14        <sup>†</sup> King Abdullah University of Science and Technology (KAUST), Biological and Environmental Science and  
15        Engineering Division, Advanced Membranes and Porous Materials Center, 23955-6900, Thuwal, Saudi Arabia.

## 16        **Abstract**

17        Nanostructured (hybrid) membranes combining properties of inorganic and polymeric materials is an  
18        integral part of the field of separation technology. Mixed matrix membranes were prepared from  
19        oppositely charged inorganic (INPs) and polymeric (PNPs) nanoparticles using spin coating method. Four  
20        different types of PNPs were prepared. Poly(2-dimethylaminoethyl methacrylate)-*b*-(methyl  
21        methacrylate)) and poly((methacrylic acid)-*b*-(methyl methacrylate)) diblock copolymers were prepared  
22        via RAFT dispersion polymerization in ethanol at 70°C. Quaternized poly(2-(dimethylamino) ethyl

23 methacrylate)-*b*-poly (benzyl methacrylate) and poly(potassium 3-sulfopropyl methacrylate)-*b*-poly  
24 (benzyl methacrylate) block copolymers were prepared using aqueous RAFT emulsion polymerization  
25 method at 70°C. The inorganic iron oxide nanoparticles (INPs) were either coated with [3-(2-  
26 Aminoethylamino)propyl] trimethoxysilane (TPED) via Dimercaptosuccinic acid (DMSA) using stab  
27 exchange. Transmission electron microscopy (TEM) and Dynamic light scattering (DLS) analysis were  
28 performed to examine the size and morphology of the prepared polymeric and inorganic nanoparticles.  
29 Scanning electron microscope (SEM) and Atomic Force Microscope (AFM) images were obtained to  
30 analyze the topography and thin film formation on the nylon support. Detailed filtration experiments were  
31 carried out to evaluate the effect of pH on the performance of the membrane.

32 **Keywords:** pH-responsive membranes, Block copolymer nanoparticles, Iron oxide nanoparticles,  
33 Surface charge, SEM, AFM, Filtration

## 34        **1. Introduction**

35        Since the last few decades, polymeric membranes have played an essential role in separation and  
36        purification technologies. However, there are certain limitations of these membranes posed by their  
37        mechanical stability, particularly for thin-film membranes, and chemical resistant [1]. Mixed matrix  
38        membranes have been evolved as a potential alternative to polymeric membranes because of their  
39        superior mechanical properties by choosing suitable components [2, 3]. The fabrication method for such  
40        composite membranes consists of incorporation of inorganic nanoparticles into a polymeric matrix.  
41        Several types of inorganic materials have been reported so far in the literature to prepare these hybrid  
42        membranes including mesoporous materials [4], carbon nanotubes (CNTs) [5], zeolites [6, 7], metal-  
43        organic frameworks (MOFs) [8], and metal oxides [9, 10]. The most exciting feature of these hybrid  
44        membranes is that they exhibit merits of both phases (organic and inorganic materials), such as  
45        mechanical stability and pressure resistance comes from inorganic phase while flexibility, low cost, and  
46        processability results from the polymeric material [11]. Apart from giving higher mechanical stability, the  
47        incorporation of nanoparticles also provides other unusual characteristics such as photochemical,  
48        magnetic and antimicrobial properties, which results in advanced applications of such hybrid membranes  
49        [12].

50        A critical challenge for the advancement of membranes is to have higher permeability and reasonable  
51        selectivity in a single membrane. This challenge comes with the requirement of selective and thin-film  
52        membranes in addition to the high porosity and regular porous structure [13]. Amphiphilic block  
53        copolymers have gained so much attraction, as a potential solution to challenges mentioned above  
54        because of their capability to self-assemble into ordered nanostructures, i.e., porous materials [14, 15].  
55        Pore size and structure of membrane can easily be tuned by playing with the type and morphology of  
56        block copolymers, which eventually tunes the flux, and the selectivity of the membranes. These  
57        fascinating self-assembling copolymers have increased the scope of application such as purification in  
58        food and pharmaceutical industry [16], water treatment [17], drug delivery [18], data storage [19] and

59 hemodialysis [20]. So far, different methods including extrusion, spin coating, and bulk evaporation have  
60 been developed to prepare membranes from block copolymers [21]. The major drawback of these  
61 methods is the requirement of post-fabrication steps to make porous structures in the thin films. Recently,  
62 this problem has been solved by combining two phenomena, self-assembly of block copolymers with the  
63 non-solvent induced phase separation (NIPS), to produce exceptionally isoporous asymmetric membranes  
64 without the need of any post-fabrication step to create porosity [22].

65 Recently, stimuli-responsive membranes have gained attention due to their switchable physicochemical  
66 and barrier properties [23]. These new membranes can modify their mass transfer and interfacial  
67 properties in response to the external stimuli including direct ones (i.e., pH, temperature and ionic  
68 strength [24, 25]) and newly developed remote or indirect triggers (i.e., light, magnetic and electric fields  
69 [26, 27]). The main objective for the preparation of stimuli-responsive membranes is to have the  
70 reversible changes in addition to the high selectivity at a faster rate. The conformational changes in the  
71 functional groups of responsive polymers, either in bulk membrane or at the surface, give rise to the  
72 stimulus response. The process of responsiveness in such membranes usually occurs in two steps [28]: (i)  
73 morphological changes in polymer, on microscopic level, in response to the stimuli (ii) intensification of  
74 these microscopic morphological transformations into macroscopic changes that can be measured as  
75 different membrane properties. As compared to other external stimuli, pH responsiveness provides more  
76 alternatives for materials and their application fields, making it a new and useful approach.

77 Zhang et al. [29] described the production of pH-sensitive membranes by mixing ethylcellulose with  
78 poly(N-isopropyl acrylamide-co-methacrylic acid) nanoparticles, produced via aqueous dispersion  
79 polymerization method. The prepared membranes were coated with the layers of polyelectrolyte to  
80 prevent the separation of nanoparticles from the membrane surface. Nunes et al. [30] prepared the pH-  
81 responsive membranes having self-assembly of metal-block copolymer complexes using NIPS technique.  
82 The structure of the thin film was manipulated by using different stability constants of series of metal-  
83 polymer complexes. The most vigorous pH response was evident for the membranes having pores of

84 nano-meter size. The effect of pH on the pore sizes of hybrid membranes was also reported by Tufani et  
85 al. [31]. These composite membranes were synthesized by the surface modification of the pore walls with  
86 pH-responsive block copolymer via initiated chemical vapor deposition (iCVD). pH responsiveness of the  
87 prepared membranes was tested under various pH values by using different permeates such as polyacrylic  
88 acid (PAA), nanoparticles, and BSA protein. Recently, Fan et al. [32] reported the development of pH  
89 sensitive smart gating membranes by efficiently incorporating poly(*N,N'*-dimethylamino-2-ethyl  
90 methacrylate) (PDMAEMA) microgels, as functional gates, into poly(ether sulfone) (PES) membrane  
91 through liquid-induced phase separation technique. The prepared membranes displayed positive pH-  
92 responsive behavior in an acidic environment whereas in a basic environment, negative pH-responsive  
93 behavior was evident.

94 Recently, we developed a novel method to synthesize thin-film membranes from sequential spray coating  
95 of self-assembled block copolymers nanoparticles [33]. Spray coating is a convenient approach to prepare  
96 thin layers involving two mechanisms, bulk movement in the spray and random spreading in the liquid  
97 film [34]. The anionic and cationic block copolymers were produced using Reversible Addition  
98 Fragmentation Chain Transfer (RAFT) aqueous emulsion polymerization method which, self-assembled  
99 spontaneously into spherical nanoparticles in the presence of water through polymerization induced self-  
100 assembly. The results revealed the fine-tuning of polymeric layer thickness by controlling the number of  
101 deposited layers. Formation of porous and defect free membranes was also confirmed by imaging  
102 analysis. In our previous studies [14, 35-37], we also reported the preparation of nanocomposite  
103 membranes with particular pore sizes, by using already produced colloidal stable solutions. By  
104 movement using this method, membrane of desired pore size could be easily synthesized by first  
105 preparing the nanoparticles of a particular diameter which will assemble to give a porous membrane with  
106 the desired properties. The final properties of the developed membranes were also manipulated by playing  
107 with the type of nanoparticles [14, 37]. We reported the preparation of nanocomposite membranes from  
108 block copolymer nanoparticles of different morphologies (worms, spheres, and vesicles) and

109 functionalized iron oxide nanoparticles [36]. The results showed a prominent effect of the amount of  
110 functionalized INPs and pH values on the mechanical stability of membranes. Application of the  
111 magnetic field also showed an increase in the flux due to the movement of the magneto-responsive iron  
112 oxide nanoparticles [37].

113 In this study, new strategies to prepare inorganic nanoparticles (INPs) and polymeric nanoparticles having  
114 positive and negative surface charges are being developed. Thin-film membranes are synthesized by the  
115 combination of positive inorganic nanoparticles (INPs) coated with [3-(2-Aminoethylamino)propyl]  
116 trimethoxysilane (TPED) and negative diblock copolymeric nanoparticles (PNPs) such as PMAA<sub>64</sub>-  
117 PMMA<sub>400</sub> and by combining negative INPs coated with Dimercaptosuccinic acid (DMSA) and positive  
118 PNPs (PDMAEMA<sub>80</sub>-PMMA<sub>500</sub>). Another set of polymeric nanoparticles having positive and negative  
119 surface charges (PQDMA<sub>23</sub>-PBzMA<sub>300</sub> and PKSPMA<sub>36</sub>-PBzMA<sub>300</sub>), previously prepared in our group  
120 [33], is also mixed with inorganic nanoparticles coated with the opposite charges to make thin-film  
121 membranes. In contrast to our previous studies, functionalization of INPs is done on the core of the  
122 particle instead of a polymeric chain on the surface. Furthermore, pH-sensitive (PMAA and PDMAEMA)  
123 and non-pH-sensitive (PQDMA and PKSPMA) block copolymer nanoparticles are utilized in this study to  
124 assess the effect of pH on the membrane performance. Using these four types of PNPs along with the two  
125 pH sensitive INPs allow preparation of membranes from PNP/ INP pairs where both nanoparticles are  
126 sensitive to pH as well as pairs that only the INP has pH sensitivity. This large combination of  
127 nanoparticles permits the preparation of pH sensitive membranes with different pore sizes and flux  
128 values. The nanoparticles are characterized by Transmission Electron Microscopy (TEM) and Dynamic  
129 Light Scattering (DLS). Nanocomposite membranes are analyzed by using Atomic Force Microscopy  
130 (AFM), Scanning Electron Microscopy (SEM), and filtration tests at different pH values.

## 131 **2. Results and discussion**

### 132 **2.1. Synthesis and characterization of the block copolymer nanoparticles (PNPs) and** 133 **inorganic nanoparticles (INPs)**

134 In our previous study [36], we synthesized mixed matrix membranes from negatively charged PMAA-*b*-  
135 PMMA block copolymer particles with different morphologies (prepared through polymerization induced  
136 self-assembly) and positively charged iron oxide nanoparticles coated with quaternized poly(2-  
137 dimethylamino)ethyl methacrylate. The effect of particle morphology (spheres, worms, and vesicles),  
138 added amount of inorganic particles and pH values on filtration and mechanical performance of the  
139 prepared membranes were evaluated. It was demonstrated that the membranes from spherical NPs in the  
140 presence of high enough positively charged magnetic nanoparticles had the best performance with a pore  
141 size of 2–20 nm. The positively charged INPs increased the mechanical stability of the final membrane  
142 due to electrostatic attractions.

143 In this work, following a similar methodology, a library of charged spherical polymeric nanoparticles  
144 (pH-responsive and non-pH responsive) is prepared. Reversible Addition Fragmentation Chain Transfer  
145 (RAFT) ethanolic dispersion and aqueous emulsion polymerization methods are used to synthesize  
146 positively and negatively charged diblock copolymer nanoparticles through polymerization induced self-  
147 assembly (PISA) method. The cationic diblock copolymer particles are synthesized by using cationic  
148 steric stabilizer (macro-chain transfer agent) based on poly(2-dimethylaminoethyl methacrylate)  
149 (PDMAEMA), and a core-forming hydrophobic block based on poly(methyl methacrylate) (PMMA). The  
150 second cationic block copolymer nanoparticles are prepared by using a macro-chain transfer agent based  
151 on quaternized poly(2-(dimethylamino) ethyl methacrylate) (PQDMA), and a hydrophobic core based on  
152 poly(benzyl methacrylate) (PBzMA). On the other hand, the anionic diblock copolymer nanoparticles are  
153 prepared using an anionic stabilizer of PMAA, and a hydrophobic core of PMMA. Similarly, the second  
154 anionic copolymer nanoparticles were made from an anionic poly(potassium 3-sulfopropyl methacrylate)  
155 (PKSPMA) stabilizer and a hydrophobic core of PBzMA. All four block copolymer nanoparticles formed  
156 spherical nanoparticles in ethanol or water under polymerization induced self-assembly (PISA) regime.

157 DLS study of PDMAEMA<sub>80</sub>-PMMA<sub>500</sub> nanoparticles presented broad size distribution and stable spheres  
158 with an average hydrodynamic diameter of  $28.8 \pm 1.3$  nm with the polydispersity index of 0.9 and width  
159 of  $25.5 \pm 0.3$  nm (from TEM analysis) (Fig. S1C). DLS investigation of PMAA<sub>64</sub>-PMMA<sub>400</sub> nanoparticles



160 also indicated narrow size distribution, and stable spheres with an average hydrodynamic diameter of 22.8  
161  $\pm 1.7$  nm, the diameter of these nanoparticles from TEM investigation is about  $18.9 \pm 1.1$  nm (Fig. S1D).  
162 Furthermore, PMAA<sub>64</sub>-PMMA<sub>400</sub> bearing negative surface charge, due to the presence of polymethacrylic  
163 acid groups on their surface, with a zeta potential of  $-38 \pm 2.0$  mV at pH 8. The PDMAEMA<sub>80</sub>-PMMA<sub>500</sub>  
164 particles had positive surface charge (zeta potential value of  $28.9 \pm 5.0$  mV at pH 8 (Table S1)) due to the  
165 presence of the amine groups. DLS measurements of PQDMA<sub>23</sub>-PBzMA<sub>300</sub> nanoparticles revealed narrow  
166 size distribution and stable spheres with an average hydrodynamic diameter of 40 nm whereas a narrow  
167 size distribution and stable spheres with an average hydrodynamic diameter of 45 nm were obtained for  
168 PKSPMA<sub>36</sub>-PBzMA<sub>300</sub> nanoparticles. TEM analysis showed a diameter of  $26.4 \pm 1.1$  nm and  $28.8 \pm 0.5$   
169 nm for PQDMA<sub>23</sub>-PBzMA<sub>300</sub> and PKSPMA<sub>36</sub>-PBzMA<sub>300</sub> nanoparticles, respectively (Figs. S1E & S1F).  
170 The charged inorganic nanoparticles were synthesized via previously reported methods [39, 40].  
171 Positively charged iron oxide nanoparticles bearing amino groups (INPs-TPED), and the negatively charged  
172 particles had succinic acid groups on their surface (INPs-DMSA) (Fig. 1). DLS measurements of INPs-  
173 TPED nanoparticles showed narrow size distribution and solid spheres having an average hydrodynamic  
174 diameter of 57.4 nm. The TEM analysis of the nanoparticles proposed diameter of 3.1 nm (Fig. S1A).  
175 DLS characterization of INPs-DMSA also displayed narrow size distribution and stable spheres with an  
176 average hydrodynamic diameter of 25.4 nm, whereas the diameter from TEM analysis was 1.0 nm (Fig.  
177 S1B).

178

## 179 **2.2.Synthesis and Characterization of Hybrid Membranes**

180 To prepare the casting solutions, oppositely charged PNP and INP were mixed at different ratios (Fig. 1).  
181 To avoid precipitation of the oppositely charged nanoparticles, the isoelectric point (IEP) of each  
182 PNP/INP pair was determined, and the PNP: INP ratios were kept below the IEP of each pair (see Table  
183 1). The casting solution mixtures were stirred at room temperature for 24h. This solution mixture was  
184 then vortexed 10-15 minutes before membrane casting. Spin coating was used to deposit a thin layer of

185 the nanoparticles on commercial nylon support with an average pore diameter of 0.2  $\mu\text{m}$ . The prepared  
186 hybrid membranes were analyzed using AFM, SEM and filtration test.

187 **Table 1.** Summary of amounts of nanoparticles required for preparation of the membrane casting solutions

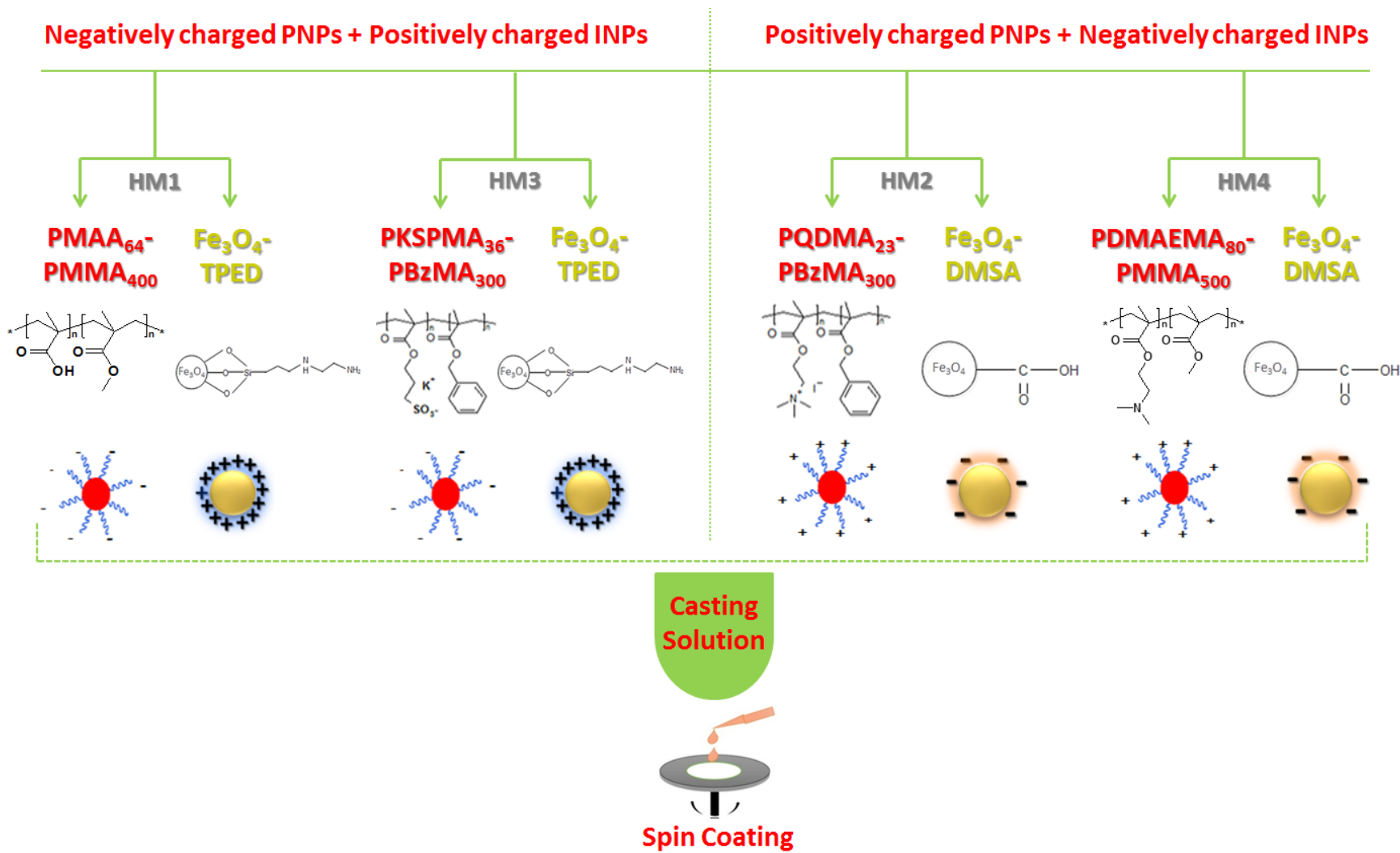
Sample ID	Sample Membranes	Inorganic Nanoparticles (INPs)*				Polymeric Nanoparticles (PNPs)			
		Amount of INPs to get the isoelectric point (mL)		Amount of INPs to get the isoelectric point (mL)		Amount of PNPs to make membrane solution (mL)			
		Fe <sub>3</sub> O <sub>4</sub> -DMSA	Fe <sub>3</sub> O <sub>4</sub> -TPED	Fe <sub>3</sub> O <sub>4</sub> -DMSA	Fe <sub>3</sub> O <sub>4</sub> -TPED	PDMAEMA <sub>80</sub> -PMMA <sub>500</sub>	PMAA <sub>64</sub> -PMMA <sub>400</sub>	PQDMA <sub>23</sub> -PBzMA <sub>300</sub>	PKSPMA <sub>36</sub> -PBzMA <sub>300</sub>
<b>HM1</b>	PMAA <sub>64</sub> -PMMA <sub>400</sub> -Fe <sub>3</sub> O <sub>4</sub> -TPED	-	1.4	1.2	-	-	0.5	-	-
<b>HM2</b>	PQDMA <sub>23</sub> -PBzMA <sub>300</sub> -DMSA-Fe <sub>3</sub> O <sub>4</sub>	3.0	-	-	2.6	-	-	0.5	-
<b>HM3</b>	PKSPMA <sub>36</sub> -PBzMA <sub>300</sub> -TPED-Fe <sub>3</sub> O <sub>4</sub>	-	2.6	2.0	-	-	-	-	0.5
<b>HM4</b>	PDMAEMA <sub>80</sub> -PMMA <sub>500</sub> -Fe <sub>3</sub> O <sub>4</sub> -DMSA	1.0	-	0.8	-	0.5	-	-	-

188 \* Concentration of Fe<sub>3</sub>O<sub>4</sub>-DMSA stock solution = 2.14 mg/mL

189 \* Concentration of Fe<sub>3</sub>O<sub>4</sub>-TPED stock solution = 1.27 mg/mL

190

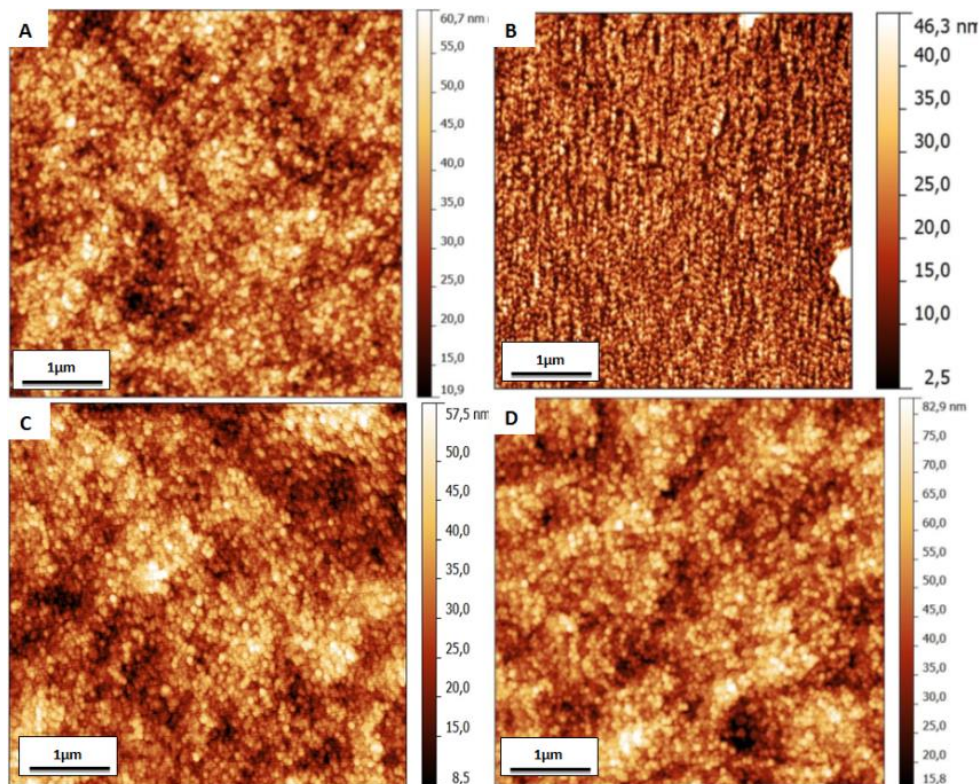
191



192

193 **Fig. 1.** Schematic representation of nanostructured membrane prepared from oppositely charged PNPs and INPs

194 Fig. 2 shows the topography of the prepared four nanostructured membranes. These AFM images clearly  
195 show the spherical morphology of the PNP nanoparticles and also confirm the compact packing of the  
196 PNPs with no visible alteration due to the presence of the INPs.

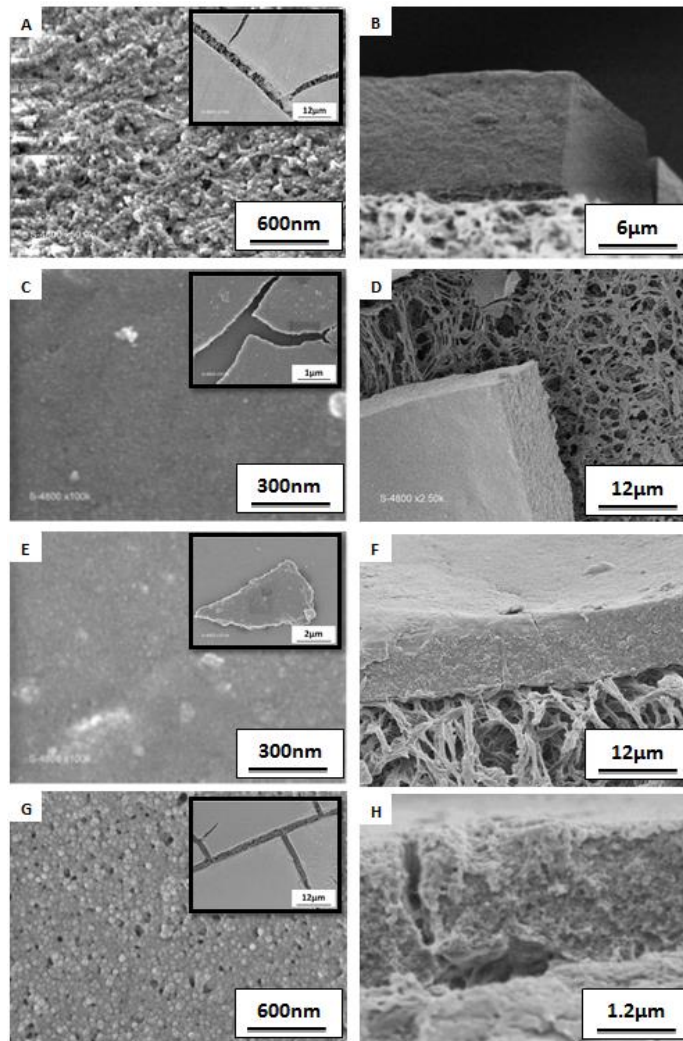


197

198 **Fig. 2.** Atomic force microscopic images of the membranes (A) **HM1** (B) **HM2** (C) **HM3** and (D) **HM4**.

199

200 The SEM images of all four membranes (**HM1-4**, Fig. 3) display the formation of defect-free active  
201 layers. The thickness of the top layer of membrane containing PMAA<sub>64</sub>-PMMA<sub>400</sub> and INPs-TPED is  
202 about 1.82 μm while membrane containing PDMAEMA<sub>80</sub>-PMMA<sub>500</sub> and INPs-DMSA has top layer  
203 thickness of 1.84 μm. Similarly, PQDMA<sub>23</sub>-PBzMA<sub>300</sub> and PKSPMA<sub>36</sub>-PBzMA<sub>300</sub> nanoparticles based  
204 membranes have top layer thickness of 1.89 μm and 1.56 μm, respectively.



205

206 **Fig. 3.** SEM images of (A, C, E, and G) top surface and (B, D, F and H) cross-section of (A, B) **HM1**, (C, D) **HM2**,  
 207 (E, F) **HM3** and (G, H) **HM4** membranes. Insets present the images of the top surface with lower magnification.

208 It is apparent that the void among the congested nanoparticles gives rise to the porous structure.

209 Theoretical pore size was estimated using a straightforward model based on the hexagonal arrangement of

210 mono-disperse spheres [35]. Here, the average diameter of the PMAA<sub>64</sub>-PMMA<sub>400</sub> and PDMAEMA<sub>80</sub>-

211 PMMA<sub>500</sub> spherical nanoparticles are 18.9 nm and 25.5 nm, respectively as measured from TEM images.

212 The calculated pore diameter is considered to be 0.4142 times of a sphere diameter (Fig. S2). The

213 estimated pore size for **HM1** membrane is 7.8 nm, while for **HM4** membrane is 10.5 nm. By performing

214 the same calculation, the estimated pore size for **HM2** membrane is 10.9 nm, whereas for **HM3** membrane

215 this value is 11.9 nm (Table 2). The pore diameter calculations were based on particle diameters measured

216 from TEM images as the membranes are at semi-dry state; hence, the particle size should be closer to dry  
 217 state rather than the hydrodynamic diameter at colloidal state. During the calculations, the INPs diameter  
 218 was not considered since they are much smaller as compared to the PNPs. HM2 to HM4 membranes  
 219 show similar pore size compared to HM1. The shells of the PNPs used in these membranes are made of  
 220 permanently charged polymeric chains (strong poly-acid and base). The presence of permanent charge in  
 221 a polymer chain forces them to be in an extended and rigid configuration rather than the entangled and  
 222 collapsed state. In the block copolymer, the extended ionic block will be much more solvated compared to  
 223 a collapsed polymeric chain resulting in the formation of more hydrated nanoparticle shell hence a bigger  
 224 nanoparticle size and pore diameter.

225 **Table 2.** Theoretical pore sizes of the prepared membranes calculated using Eq. in Fig. S4.

Sample ID	PNPs size (nm)	Pore size (nm)
HM1	18.9	7.8
HM2	26.4	10.9
HM3	28.8	11.9
HM4	25.5	10.5

226

227 The prepared membranes were also tested for pure water filtration. The filtration cycles (repeated three  
 228 times) were all performed on the same membrane. The membranes were fitted in a filtration cell with a  
 229 diameter of 2.5 cm and a volume of 10 mL. Each membrane was conditioned for 2 hours at 3.5 bar, and  
 230 then water flux was recorded to reach an equilibrium state. For filtration under pressure, the filtration cell  
 231 was filled with water and linked with a pressurized water reservoir. Upon collection of data, Darcy's law  
 232 was used to calculate the flux ( $J_v$ ) and permeability ( $L_p$ ) values using the following equations [41]:

233 
$$J_v = \frac{V_p}{t S}$$

234  
235  
236  
237  
238  
239  
240  
241  
242  
243  
244  
245  
246  
247  
248  
249  
250  
251  
252  
253  
254  
255  
256  
257

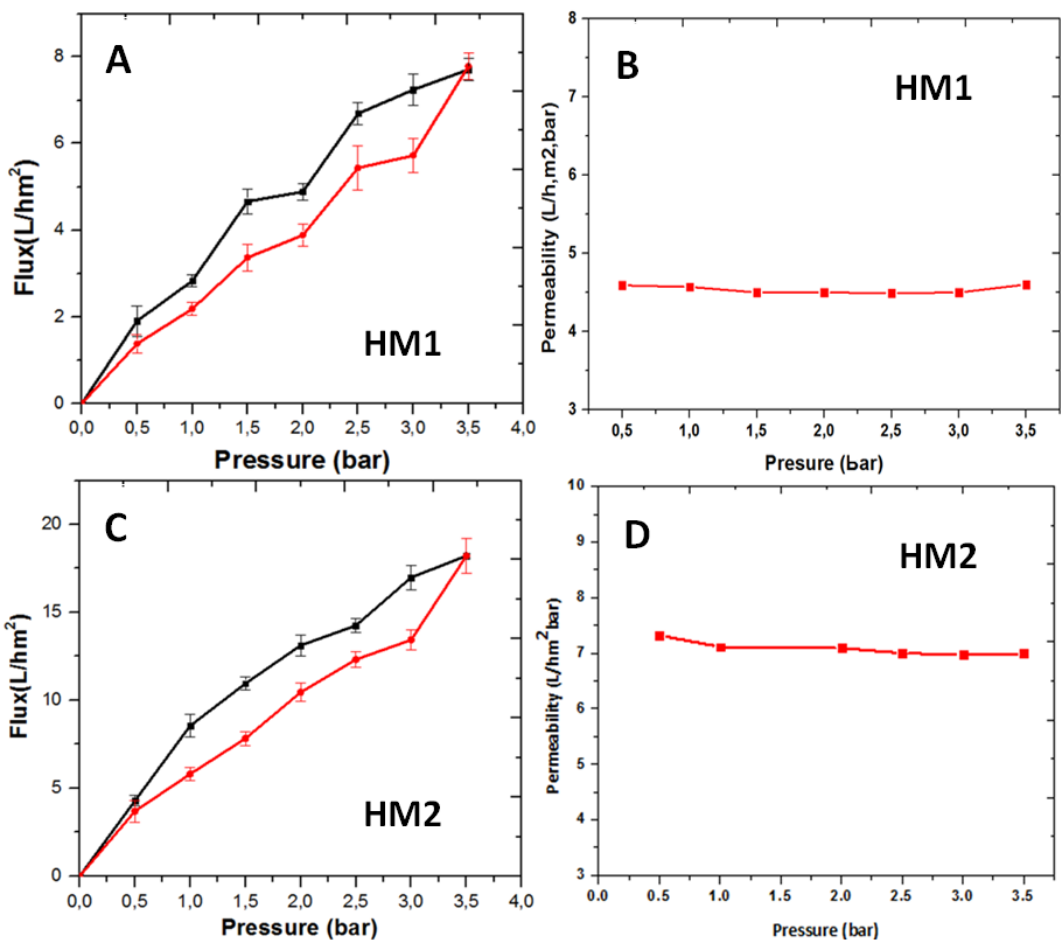
$$L_p = \frac{J_v}{\Delta P}$$

where,  $V_p$  corresponds to the volume of water going through the membrane (L),  $t$  represents time (h),  $S$  denotes the surface of the membrane ( $m^2$ ), and  $\Delta P$  is water pressure (bar).

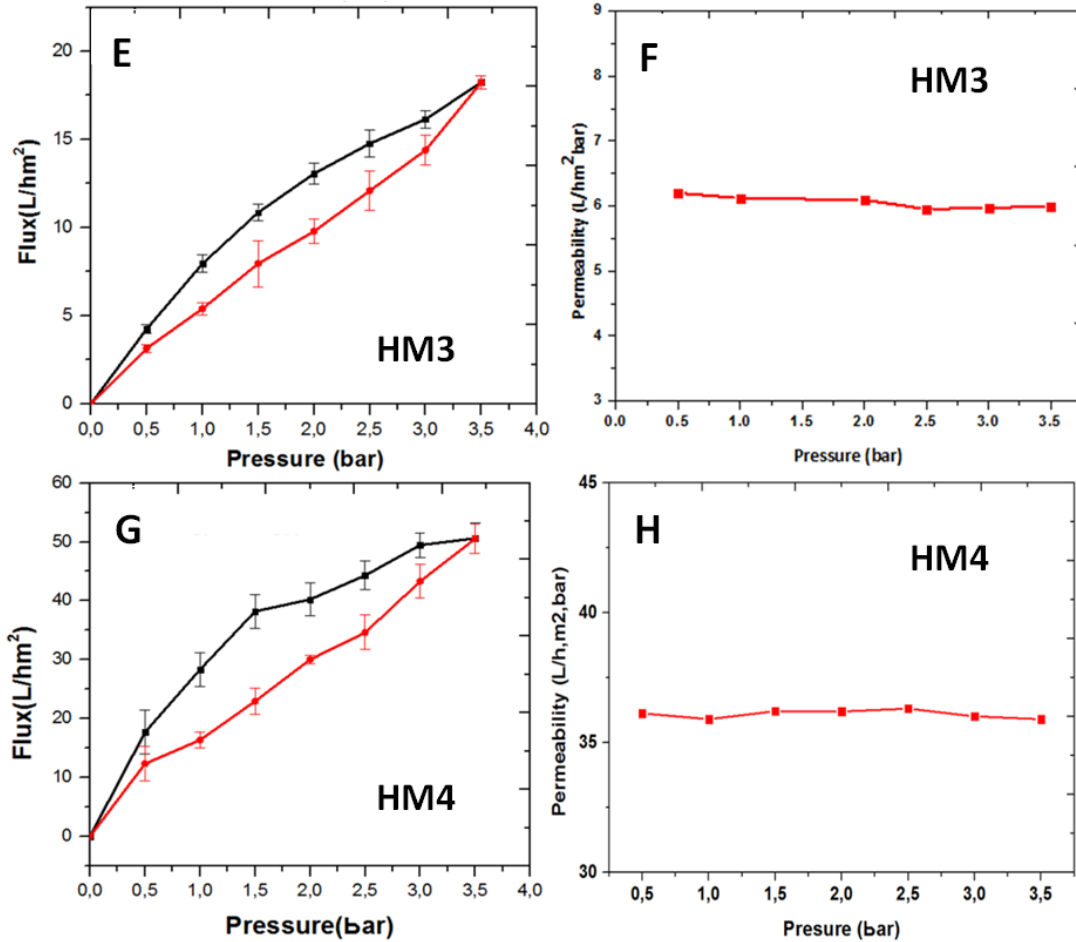
Water flux ( $J_v$ ) was calculated at different pressure intervals between 0 and 3.5 bar. At each pressure, 20 minutes equilibrium time was allowed before recording the data, followed by a 20 minutes recording. In all four cases, the water flux plots versus pressure show an almost linear increase (Figs. 5A, 4C, 4E & 5G). Figs. 5B, 5D, 5F, and 5H show that the permeability is almost constant as a function of applied pressure which also verifies the stability of the prepared membranes under tested conditions. For **HM4** membrane, at 3.5 bar the calculated flux was 50.8 L/hm<sup>2</sup> and the resultant permeability was 36.2 L/hm<sup>2</sup>bar whereas for **HM1** membrane, at 3.5 bar the calculated flux was 7.69 L/h.m<sup>2</sup>, and the resultant permeability was 4.60 L/hm<sup>2</sup>bar. In the same way, for **HM3** membrane, at 3.5 bar the calculated flux was 18.7 L/hm<sup>2</sup> with the permeability of 4.52 L/hm<sup>2</sup>bar and for **HM2** membrane, at 3.5 bar the calculated flux is 18.3 L/hm<sup>2</sup> with the permeability of 5.34 L/hm<sup>2</sup>bar. These flux values were lower than the values already reported in literature for PMAA-PMMA based membranes having PMAA-*b*-PQDMAEMA coated INPs [36, 37] which may be due to the fact that the INPs used in this study are stabilized using small molecules as compared to the INPs used in the previous study which had hairy shell structure (stabilized with positively charged polymer chains with an average size of 7 nm). These particles were less prone to aggregation because of the presence of the charged polymer chain. However, the INPs stabilized using only an acid or amine group (INP-DMSA and INP-TPED) aggregated readily as it could be seen from the data presented in Table S1. The average size measured from TEM images (dry state) show particle diameters of 1 and 3 nm for the negatively and positively charged particles respectively. While DLS measurements in solution, gave diameters of 25 and 57 nm for the same particles. Such a big difference in size could only be due to particle aggregation. Therefore, if the INPs present in the membrane dope solutions are aggregated (i.e. larger diameters) they would possibly clog some of the



258 membrane pores reducing the apparent pore size, resulting in lower flux values. This aggregation could  
259 also be the reason behind the small hysteresis observed in the flux curves. If the INPs are aggregated, they  
260 would interact less with the polymer chains stabilizing the PNPs. This could influence the cohesion of the  
261 particles brought about by the electrostatic forces due to the presence of oppositely charged nanoparticles.  
262 Weaker cohesion would lead to lower stability of the membrane active layer that could be slightly pushed  
263 into the support layer under water pressure (during filtration).



264

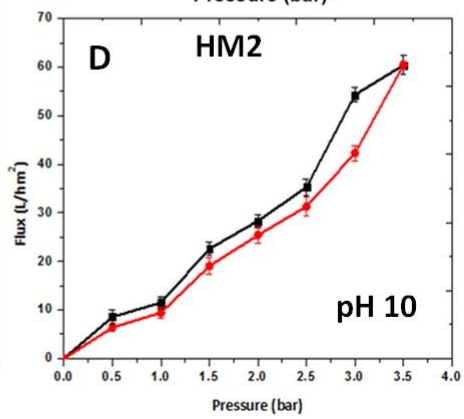
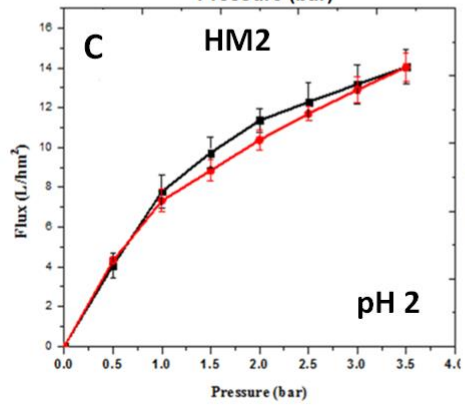
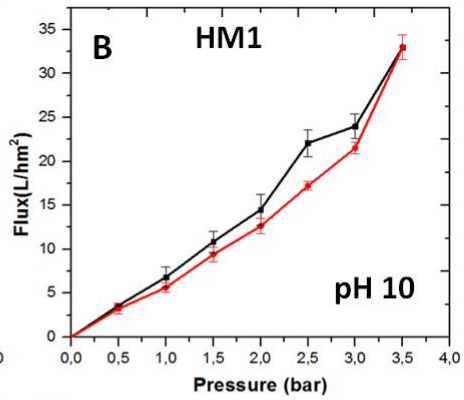
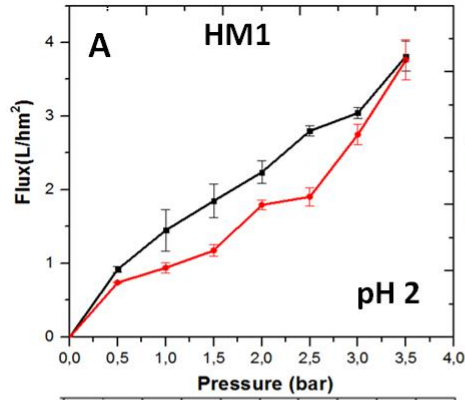


265

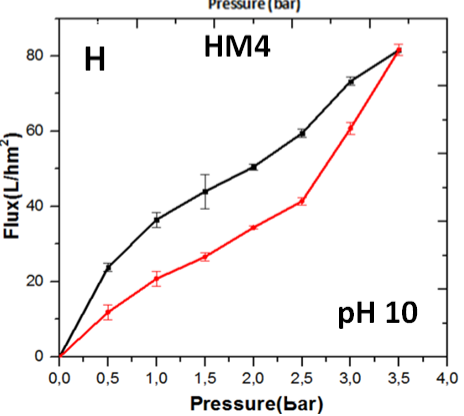
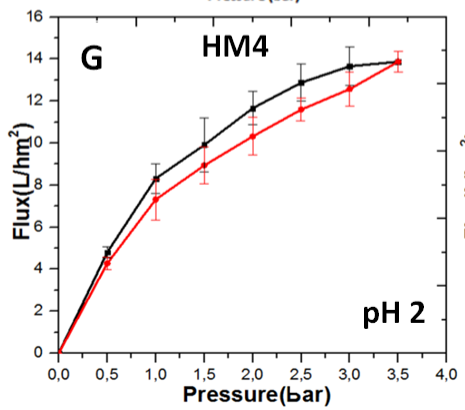
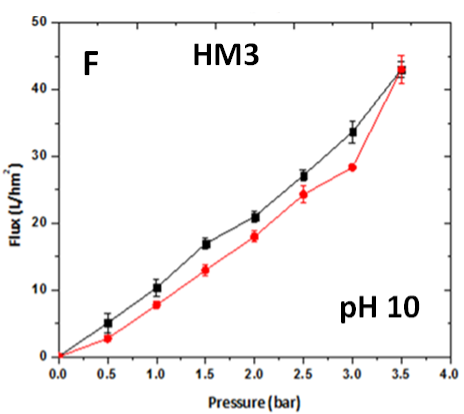
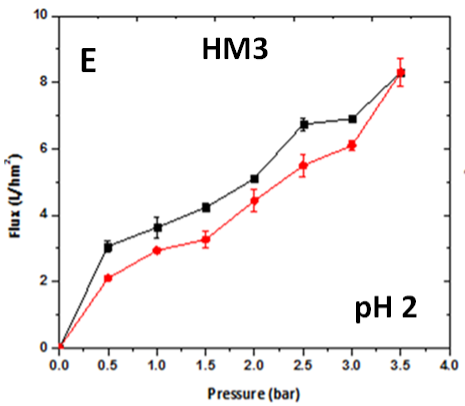
266 **Fig. 5.** (A, C, E, and G) Water flux ( $J_v$ ) and (B, D, F, and H) Permeability ( $L_p$ ) as a function of pressure for  
 267 nanostructured membranes (A, B) **HM1** (C, D) **HM2** (E, F) **HM3** and (G, H) **HM4** at pH of 7. The reported values  
 268 are the average of three different measurements, and the bars represent the standard deviation. Blackline is pressure  
 269 ramp up, and the red is the ramp down.

270

271 PMAA<sub>64</sub>-PMMA<sub>400</sub> and PDMAEMA<sub>80</sub>-PMMA<sub>500</sub> polymeric nanoparticles are pH-sensitive because of the  
 272 presence of PMAA and PDMAEMA on their surface. So are the inorganic nanoparticles used, as they  
 273 bear either -COOH (DMSA, pK<sub>a</sub> 1 = 2.9, pK<sub>a</sub> 2 = 4.5) or -NH<sub>2</sub> (TPED, pK<sub>a</sub> = 8) functionalities. To see  
 274 the effect of the pH change on the pore size of the nanostructured membranes, filtration tests at acidic and  
 275 basic pH values were performed. Feed solutions with pH values below and above the pK<sub>a</sub> of PDMAEMA  
 276 and PMAA (7.4-7.8 and 6.1, respectively) [36, 42] were used for filtration (pH 2 and 10). The flux shows  
 277 the increasing trend as a function of applied pressure for both acidic and basic pH values (Fig. 6A-H).



278



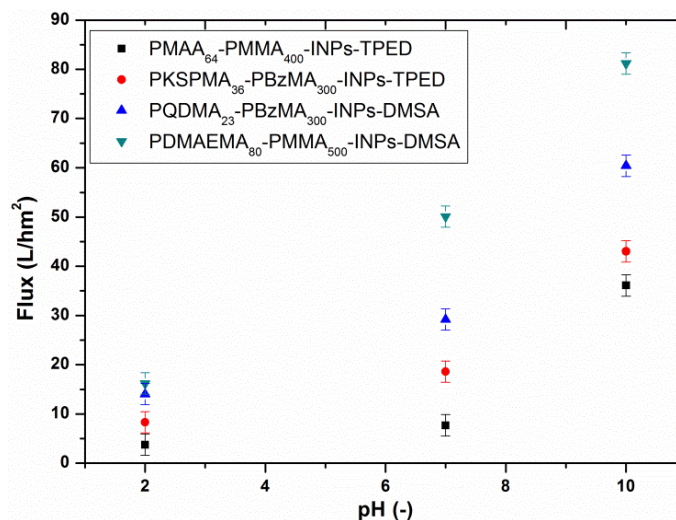
279

280 **Fig. 6.** Water flux ( $J_v$ ) as a function of pressure for (A, B) **HM1** membranes, (C, D) **HM2** membranes, (E, F) **HM3**  
281 membranes and (G, H) **HM4** membranes, at (A, C, E and G) pH 2 and (B, D, F and H) pH 10. The values are the  
282 average of three different measurements, and the bars represent the standard deviation. Blackline is pressure ramp  
283 up, and the red is a ramp down.  
284  
285

286 The flux increases progressively from 3.5 L/hm<sup>2</sup> at 1.0 bar to 34.6 L/hm<sup>2</sup> at 3.5 bar for pH 10 in case of  
287 **HM1**, while for **HM4** membrane flux increases gradually from 22.3 L/hm<sup>2</sup> at 1 bar to 81.2 L/hm<sup>2</sup> at 3.5  
288 bar for pH 10. Likewise, the flux increases from 11.5 L/hm<sup>2</sup> at 1.0 bar to 60.4 L/hm<sup>2</sup> at 3.5 bar for pH 10  
289 in case of **HM2**, whereas for **HM3** membrane flux increases from 10.33 L/hm<sup>2</sup> at 1 bar to 43.03 L/hm<sup>2</sup> at  
290 3.5 bar for pH 10. The SEM analysis of hybrid membranes was also performed after filtration tests and  
291 the micrographs revealed no signs of deformation on the active layer (Fig. S5).

292 To be able to compare the membranes together, the maximum flux values recorded at 3 different pH (2, 7  
293 and 10) at 3.5 bar were plotted in one single figure (Fig. 7). The flux values were at lowest when the  
294 water pH was 2. The flux values are lower for prepared membranes at pH 2 as compared to the values at  
295 pH 10. This is because at pH 2 there is only a small number of charges present since pH 2 is below the  
296 pKa of all the used functional nanoparticles (PNP and INP). As the number of apparent charge on the  
297 surface of the nanoparticles increase ( $\text{pH} \geq 10$ ) the flux value increases sharply. This is most likely due to  
298 the repulsive forces generated between the packed particles forcing them to move. This stands out more in  
299 membranes made from nanoparticles coated with PDMAEMA as stabilizer (with highest flux values at all  
300 3 pH values tested). For this nanoparticle pair (PDMAEMA-PMMA and INP-DMSA) there is no pH  
301 value where both particles are charged. This means that the cohesion between the PNP particles is at its  
302 minimum due to same charge repulsion.

303 The changes in flux brought about by pH could be very useful to tune the pore size according to the  
304 filtration regime/ range. If membrane with bigger pore size is required a cycle of filtration with water at  
305 pH 10 could be performed prior to the actual sample filtration. Another simple method to tune the pore  
306 size would be to soak the membrane in water with a certain pH value.



307

308 **Fig. 7.** Water flux as a function of pH for different nanostructured membranes at 3.5 bar. Black color represents  
 309 PMAA<sub>64</sub>-PMMA<sub>400</sub>-INPs-TPED (HM1 membrane), red color represents PKSPMA<sub>36</sub>-PBzMA<sub>300</sub>-INPs-TPED  
 310 (HM3 membrane), blue color represents PQDMA<sub>23</sub>-PBzMA<sub>300</sub>-INPs-DMSA (HM2 membrane) and green color  
 311 represents PDMAEMA<sub>80</sub>-PMMA<sub>500</sub>-INPs-TPED (HM4 membrane).

312

### 313 Conclusion

314 In summary, iron oxide nanoparticles were prepared by polyol method and functionalized with [3-(2-  
 315 Aminoethylamino)propyl] trimethoxysilane (TPED) and Dimercaptosuccinic acid (DMSA) to achieve the  
 316 positive and negative charges on their surface. PDMAEMA<sub>80</sub>-PMMA<sub>500</sub> and PMAA<sub>64</sub>-PMMA<sub>400</sub>  
 317 copolymer nanoparticles were prepared via RAFT-PISA synthesis method in ethanol while PKSPMA<sub>36</sub>-  
 318 PBzMA<sub>300</sub> and PQDMA<sub>23</sub>-PBzMA<sub>300</sub> copolymer nanoparticles in water. High conversions were attained  
 319 within 24 hours. DLS analysis showed their spherical features, and TEM images represented well-defined  
 320 nanoparticles. Cationic and anionic nanoparticle pairs were effectively utilized to synthesize thin-film  
 321 membranes by spin coating method on a nylon support. SEM and AFM analysis revealed the formation of  
 322 porous and defect-free membranes. Pressure-driven water filtration tests, using prepared membranes,  
 323 were performed at different pH values. Since the pK<sub>a</sub> value of polymethacrylic acid (PMAA) on the  
 324 surface of PNPs is about 6.1 and for PDMAEMA on the surface is in the range of 7.4-7.8, therefore, feed  
 325 solutions of two different pH values, 2 and 10, were used and the filtration experiments were performed.  
 326 For neutral pH (7), the membranes HM1 displayed the flux of 7.69 L/hm<sup>2</sup>, while HM4 membranes

327 showed the flux of 50.8 L/hm<sup>2</sup> at 3.5 bar of pressure. In the same way, for HM3 membranes, at 3.5 bar,  
328 the flux was 15.4 L/hm<sup>2</sup> and for HM2 membranes, at 3.5 bars, the calculated flux was 21.3 L/hm<sup>2</sup>. The  
329 highest recorded flux was 81.2 L/hm<sup>2</sup> for HM4 nanostructured membranes at the pressure of 3.5 bars and  
330 pH 10, which was linked with the deprotonation of the amine groups resulted in higher water flux. When  
331 the pH value was below the pK<sub>a</sub> value (pH 2) lower flux values were observed for all the investigated  
332 membranes which were attributed to the existence of a fewer number of charges for interaction. The  
333 filtration tests also verified the mechanical stability of studied membranes under the investigated pressure  
334 range (0-3.5 bars). The prepared nanostructure membranes were found to have a pore size in a nano-  
335 metric range following lower limit of ultrafiltration and upper limit of nano-filtration. The adequate  
336 bonding of positively and negatively charged particles (PNPs and INPs) resulted in the enhanced  
337 mechanical stability of the prepared membranes. In future work, the magneto-responsive behavior of  
338 these hybrid membranes can further be examined.

### 339 **Acknowledgments**

340 U. F. acknowledges the financial support from EM3E Master Programme, which is an Educational  
341 Programme supported by the European Commission, the European Membrane Society (EMS), the  
342 European Membrane House (EMH), and an extensive international network of industrial companies,  
343 research centers and universities. The authors would like to thank Dr. Reyes Mallada for the fruitful  
344 discussions and for the help in preparing this manuscript.

345 **References**

- 346 [1] D.J. Kim, M.J. Jo, S.Y. Nam, A review of polymer–nanocomposite electrolyte membranes for fuel  
347 cell application, *Journal of Industrial and Engineering Chemistry*, 21 (2015) 36-52.
- 348 [2] A.K. Singh, P. Singh, S. Mishra, V.K. Shahi, Anti-biofouling organic-inorganic hybrid membrane for  
349 water treatment, *Journal of Materials Chemistry*, 22 (2012) 1834-1844.
- 350 [3] Y. Gu, R.M. Dorin, U. Wiesner, Asymmetric organic–inorganic hybrid membrane formation via block  
351 copolymer–nanoparticle co-assembly, *Nano letters*, 13 (2013) 5323-5328.
- 352 [4] B. Zornoza, C. Téllez, J. Coronas, Mixed matrix membranes comprising glassy polymers and  
353 dispersed mesoporous silica spheres for gas separation, *Journal of Membrane Science*, 368 (2011) 100-  
354 109.
- 355 [5] P. Goh, A. Ismail, B. Ng, Carbon nanotubes for desalination: Performance evaluation and current  
356 hurdles, *Desalination*, 308 (2013) 2-14.
- 357 [6] M. Jia, K.-V. Peinemann, R.-D. Behling, Molecular sieving effect of the zeolite-filled silicone rubber  
358 membranes in gas permeation, *Journal of Membrane Science*, 57 (1991) 289-292.
- 359 [7] H.H. Yong, H.C. Park, Y.S. Kang, J. Won, W.N. Kim, Zeolite-filled polyimide membrane containing  
360 2, 4, 6-triaminopyrimidine, *Journal of Membrane Science*, 188 (2001) 151-163.
- 361 [8] S. Basu, A. Cano-Odena, I.F. Vankelecom, MOF-containing mixed-matrix membranes for CO<sub>2</sub>/CH<sub>4</sub>  
362 and CO<sub>2</sub>/N<sub>2</sub> binary gas mixture separations, *Separation and Purification Technology*, 81 (2011) 31-40.
- 363 [9] P. Jian, H. Yahui, W. Yang, L. Linlin, Preparation of polysulfone–Fe<sub>3</sub>O<sub>4</sub> composite ultrafiltration  
364 membrane and its behavior in magnetic field, *Journal of Membrane Science*, 284 (2006) 9-16.
- 365 [10] S. Matteucci, V.A. Kusuma, D. Sanders, S. Swinnea, B.D. Freeman, Gas transport in TiO<sub>2</sub>  
366 nanoparticle-filled poly (1-trimethylsilyl-1-propyne), *Journal of Membrane Science*, 307 (2008) 196-217.
- 367 [11] M.M. Pendergast, E.M. Hoek, A review of water treatment membrane nanotechnologies, *Energy &*  
368 *Environmental Science*, 4 (2011) 1946-1971.
- 369 [12] P. Madhavan, P.-Y. Hong, R. Sougrat, S.P. Nunes, Silver-enhanced block copolymer membranes  
370 with biocidal activity, *ACS applied materials & interfaces*, 6 (2014) 18497-18501.
- 371 [13] G. Dong, H. Li, V. Chen, Challenges and opportunities for mixed-matrix membranes for gas  
372 separation, *Journal of Materials Chemistry A*, 1 (2013) 4610-4630.
- 373 [14] L. Upadhyaya, M. Semsarilar, R. Fernández-Pacheco, G. Martinez, R. Mallada, A. Deratani, D.  
374 Quemener, Porous membranes from acid decorated block copolymer nano-objects via RAFT alcoholic  
375 dispersion polymerization, *Polymer Chemistry*, 7 (2016) 1899-1906.
- 376 [15] L. Upadhyaya, M. Semsarilar, S. Nehache, A. Deratani, D. Quemener, Filtration membranes from  
377 self-assembled block copolymers—a review on recent progress, *The European Physical Journal Special*  
378 *Topics*, 224 (2015) 1883-1897.
- 379 [16] S.Y. Yang, J.-A. Yang, E.-S. Kim, G. Jeon, E.J. Oh, K.Y. Choi, S.K. Hahn, J.K. Kim, Single-file  
380 diffusion of protein drugs through cylindrical nanochannels, *Acs Nano*, 4 (2010) 3817-3822.
- 381 [17] M.A. Shannon, P.W. Bohn, M. Elimelech, J.G. Georgiadis, B.J. Marinas, A.M. Mayes, Science and  
382 technology for water purification in the coming decades, *Nature*, 452 (2008) 301-310.
- 383 [18] E.A. Jackson, M.A. Hillmyer, Nanoporous membranes derived from block copolymers: from drug  
384 delivery to water filtration, *ACS nano*, 4 (2010) 3548-3553.
- 385 [19] T. Thurn-Albrecht, J. Schotter, G. Kästle, N. Emley, T. Shibauchi, L. Krusin-Elbaum, K. Guarini, C.  
386 Black, M. Tuominen, T. Russell, Ultrahigh-density nanowire arrays grown in self-assembled diblock  
387 copolymer templates, *Science*, 290 (2000) 2126-2129.
- 388 [20] I. Hamley, Nanostructure fabrication using block copolymers, *Nanotechnology*, 14 (2003) R39-R54.
- 389 [21] D. Wu, F. Xu, B. Sun, R. Fu, H. He, K. Matyjaszewski, Design and preparation of porous polymers,  
390 *Chemical reviews*, 112 (2012) 3959-4015.
- 391 [22] S.P. Nunes, A. Car, From charge-mosaic to micelle self-assembly: block copolymer membranes in  
392 the last 40 years, *Industrial & Engineering Chemistry Research*, 52 (2012) 993-1003.
- 393 [23] C. Zhao, S. Nie, M. Tang, S. Sun, Polymeric pH-sensitive membranes—a review, *Progress in*  
394 *Polymer Science*, 36 (2011) 1499-1520.

395 [24] S. Frost, M. Ulbricht, Thermoresponsive ultrafiltration membranes for the switchable permeation and  
396 fractionation of nanoparticles, *Journal of membrane science*, 448 (2013) 1-11.

397 [25] T. Ito, T. Hioki, T. Yamaguchi, T. Shinbo, S.-i. Nakao, S. Kimura, Development of a molecular  
398 recognition ion gating membrane and estimation of its pore size control, *Journal of the American*  
399 *Chemical Society*, 124 (2002) 7840-7846.

400 [26] T. Hoare, B.P. Timko, J. Santamaria, G.F. Goya, S. Irusta, S. Lau, C.F. Stefanescu, D. Lin, R.  
401 Langer, D.S. Kohane, Magnetically triggered nanocomposite membranes: a versatile platform for  
402 triggered drug release, *Nano letters*, 11 (2011) 1395-1400.

403 [27] B.P. Timko, T. Dvir, D.S. Kohane, Remotely triggerable drug delivery systems, *Advanced materials*,  
404 22 (2010) 4925-4943.

405 [28] D. Wandera, S.R. Wickramasinghe, S.M. Husson, Stimuli-responsive membranes, *Journal of*  
406 *Membrane Science*, 357 (2010) 6-35.

407 [29] K. Zhang, H. Huang, G. Yang, J. Shaw, C. Yip, X.Y. Wu, Characterization of nanostructure of  
408 stimuli-responsive polymeric composite membranes, *Biomacromolecules*, 5 (2004) 1248-1255.

409 [30] S.P. Nunes, A.R. Behzad, B. Hooghan, R. Sougrat, M. Karunakaran, N. Pradeep, U. Vainio, K.-V.  
410 Peinemann, Switchable pH-responsive polymeric membranes prepared via block copolymer micelle  
411 assembly, *ACS nano*, 5 (2011) 3516-3522.

412 [31] A. Tufani, G.O. Ince, Smart membranes with pH-responsive control of macromolecule permeability,  
413 *Journal of Membrane Science*, 537 (2017) 255-262.

414 [32] X.-X. Fan, R. Xie, Q. Zhao, X.-Y. Li, X.-J. Ju, W. Wang, Z. Liu, L.-Y. Chu, Dual pH-responsive  
415 smart gating membranes, *Journal of Membrane Science*, 555 (2018) 20-29.

416 [33] J. Ma, H.M. Andriambololona, D. Quemener, M. Semsarilar, Membrane preparation by sequential  
417 spray deposition of polymer PISA nanoparticles, *Journal of Membrane Science*, 548 (2018) 42-49.

418 [34] W.D. Mulhearn, D.D. Kim, Y. Gu, D. Lee, Facilitated transport enhances spray layer-by-layer  
419 assembly of oppositely charged nanoparticles, *Soft Matter*, 8 (2012) 10419-10427.

420 [35] Z. Mouline, M. Semsarilar, A. Deratani, D. Quemener, Stimuli responsive nanostructured porous  
421 network from triblock copolymer self-assemblies, *Polymer Chemistry*, 6 (2015) 2023-2028.

422 [36] L. Upadhyaya, M. Semsarilar, S. Nehache, D. Cot, R. Fernández-Pacheco, G. Martinez, R. Mallada,  
423 A. Deratani, D. Quemener, Nanostructured Mixed Matrix Membranes from Supramolecular Assembly of  
424 Block Copolymer Nanoparticles and Iron Oxide Nanoparticles, *Macromolecules*, 49 (2016) 7908-7916.

425 [37] L. Upadhyaya, M. Semsarilar, R. Fernández-Pacheco, G. Martinez, R. Mallada, I.M. Coelho, C.A.  
426 Portugal, J.G. Crespo, A. Deratani, D. Quemener, Nano-structured magneto-responsive membranes from  
427 block copolymers and iron oxide nanoparticles, *Polymer Chemistry*, 8 (2017) 605-614.

428 [38] M. Semsarilar, V. Ladmiraal, A. Blanazs, S.P. Armes, Cationic Polyelectrolyte-Stabilized  
429 Nanoparticles via RAFT Aqueous Dispersion Polymerization, *Langmuir*, 29 (2013) 7416-7424.

430 [39] D.A. Mbeh, L.K. Mireles, D. Stanicki, L. Tabet, K. Maghni, S. Laurent, E. Sacher, L.H. Yahia,  
431 Human alveolar epithelial cell responses to core-shell superparamagnetic iron oxide nanoparticles  
432 (SPIONs), *Langmuir*, 31 (2015) 3829-3839.

433 [40] N. Miguel-Sancho, O. Bomati-Miguel, G. Colom, J.P. Salvador, M.P. Marco, J. Santamaría,  
434 Development of Stable, Water-Dispersible, and Biofunctionalizable Superparamagnetic Iron Oxide  
435 Nanoparticles, *Chemistry of Materials*, 23 (2011) 2795-2802.

436 [41] R.W. Baker, *Membrane technology and applications*, 2nd ed., John Wiley & Sons, Ltd, 2004.

437 [42] M. Guerre, M. Semsarilar, C. Totée, G. Sillery, B. Améduri, V. Ladmiraal, Self-assembly of  
438 poly(vinylidene fluoride)-block-poly(2-(dimethylamino)ethylmethacrylate) block copolymers prepared by  
439 CuAAC click coupling, *Polymer Chemistry*, 8 (2017) 5203-5211.

440